

212305: andalusite–sillimanite pelitic migmatite, Mount Joseph (*Mount Joseph Migmatite, Marboo Formation, Western Zone, Lamboo Province, Wunaamin Miliwundi Orogen*)

Korhonen, FJ, Romano, SS, Fielding, IOH, Kelsey, DE and Hollis, JA

Location and sampling

LENNARD RIVER (SE 51-8), RICHENDA (3963)

MGA Zone 51, 724362E 8077917N

Warox Site JBHLEN000217

Sampled on 19 July 2013

This sample was collected from outcrop in the bed of the Lennard River on Napier Downs Station, about 13.6 km south-southwest of Mount Eliza, 12.5 km north of Mount Behm, and 1.4 km southeast of Mount Joseph.

Geological context

The unit sampled is the Mount Joseph Migmatite, a component of the Marboo Formation in the Western Zone of the Lamboo Province (Tyler et al., 1999; Phillips et al., 2015). The Mount Joseph Migmatite consists of psammitic and pelitic migmatite and anatectic granite formed by in situ melting of the Marboo Formation, probably driven in part by heat advected during large-scale plutonic magmatism (Tyler et al., 1999; Phillips et al., 2015). At this locality, the pelitic gneiss is migmatitic, and contains cm-scale granitic leucosomes that are concordant with the foliation and wrap around cm-scale aluminosilicate porphyroblasts (Fig. 1). Zircon from a sample of Mount Joseph Migmatite, located 1.7 km to the west, yielded an age for high-grade metamorphism of 1865 ± 4 Ma and a conservative maximum depositional age of 1873 ± 2 Ma for the sedimentary protolith (GSWA 212317, Fielding et al., 2020). A minimum age for deposition is provided by a crystallization age of 1864 ± 4 Ma for the Lennard Granite, which intrudes the Marboo Formation and Mount Joseph Migmatite (GA8759.8011, Griffin et al., 2000). Monazite from a sample of Mount Joseph Migmatite from the same locality as sample GSWA 212317 yielded an age of 1827 ± 9 Ma (GSWA 212316, Fielding et al., 2019b). The sample reported here preserves two monazite dates that can be distinguished based on petrographic setting: Group M monazite occurs within aluminosilicate porphyroblasts and surrounding coarse-grained biotite, and yielded an age of 1854 ± 4 Ma, interpreted to date the timing of aluminosilicate porphyroblast growth during high-temperature metamorphism; Group M2 monazite occurs within the biotite–fibrolite foliation that wraps around aluminosilicate porphyroblasts, and yielded an age of 1823 ± 6 Ma, interpreted to date the development of the foliation during a fluid-rich overprinting event (GSWA 212305, Fielding et al., 2019a).

Petrographic description

The sample is a pelitic migmatite, consisting of about 40–45% quartz, 35% biotite, 9% sillimanite, 5% andalusite, 3% K-feldspar, 3% plagioclase, 2% muscovite and accessory ilmenite, monazite and zircon (Fig. 2). Porphyroblasts of aluminosilicate are up to 1 cm in size and mantled by biotite (Fig. 3a,b). These porphyroblasts are mainly composed of sillimanite grains that are in optical continuity with interstitial finer grained biotite, both of which are partially surrounded by coarse-grained andalusite (Fig. 3a,b). Within some aggregates of porphyroblasts, fibrolite partially replaces sillimanite (Fig. 3a–d). Intergrown matted fibrolite and fine-grained biotite define a well-developed, pervasive foliation that wraps around the coarse aluminosilicate porphyroblasts (Fig. 3a,b). In some places, the fibrolite mats extend into biotite rims. Some coarse needles of sillimanite show a progression to fibrolite that can be followed into the fibrolite–biotite foliation (Fig. 3c,d). Foliation-parallel leucosomes are up to 1 cm thick, and are composed of quartz, K-feldspar, plagioclase, and biotite (Fig. 2). Subhedral quartz is up to 0.8 mm in size and exhibits undulose extinction. K-feldspar is up to 1 cm in size, and contains microperthite lamellae and rare round quartz

inclusions. Melanosomes are composed of quartz, coarse-grained biotite, and fine-grained fibrolite–biotite, and contain sparse corroded laths of muscovite (Fig. 3d). Biotite compositions are provided in Table 1.



Figure 1. Outcrop image for sample 212305: andalusite–sillimanite pelitic migmatite, Mount Joseph

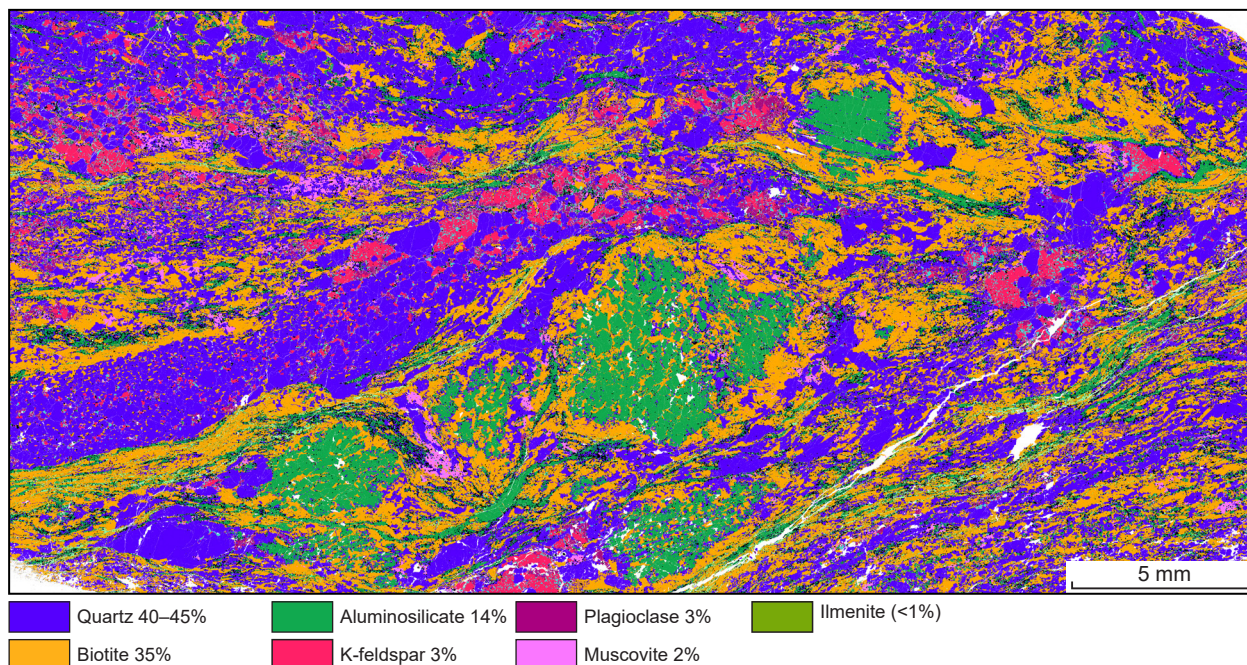


Figure 2. TESCAN Integrated Mineral Analyser (TIMA) image of an entire thin section from sample 212305: andalusite–sillimanite pelitic migmatite, Mount Joseph. Volume percent proportions of major rock-forming minerals are calculated by the TIMA software

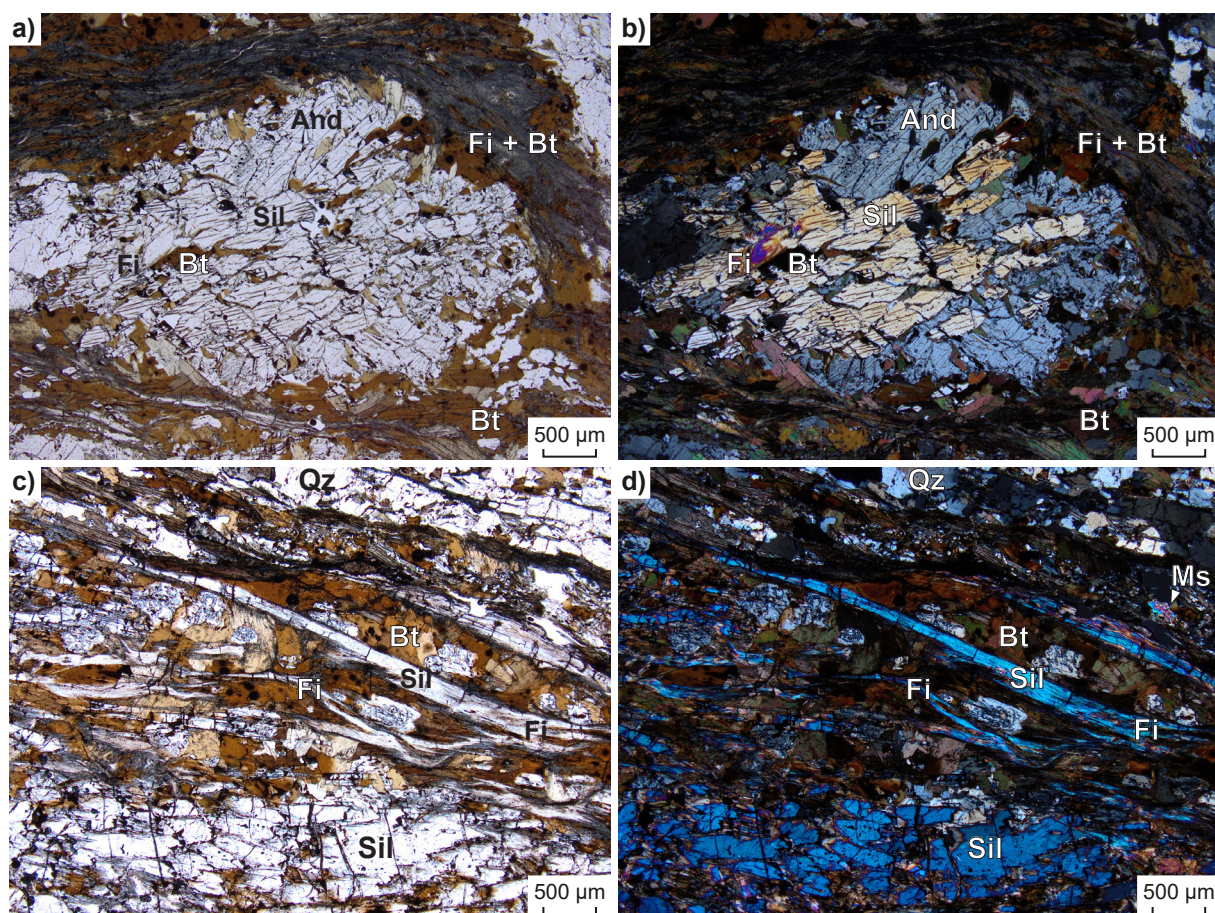


Figure 3. Photomicrographs, in plane-polarized light (a, c) and cross-polarized light (b, d), of sample 212305: andalusite-sillimanite pelitic migmatite, Mount Joseph. Mineral abbreviations are explained in the caption to Figure 4, except Fi, fibrolite

Analytical details

The metamorphic evolution of this sample was investigated using phase equilibria, based on the bulk-rock composition (Table 2). The bulk-rock composition was determined by X-ray fluorescence spectroscopy, together with loss on ignition (LOI). FeO content was analysed by Fe²⁺ titration, and Fe₂O₃ calculated by difference. The modelled O content (for Fe³⁺) was derived from the titration value; the modelled H₂O content was reduced from the measured LOI to stabilize the peak assemblage at conditions just above the solidus. Thermodynamic calculations were performed in the MnNCKFMASHTO (MnO–Na₂O–CaO–K₂O–FeO–MgO–Al₂O₃–SiO₂–H₂O–TiO₂–O) system using THERMOCALC version tc340 (updated October 2013; Powell and Holland, 1988) and the internally consistent thermodynamic dataset of Holland and Powell (2011; dataset tc-ds62, created in February 2012). The activity–composition relations used in the modelling are detailed in White et al. (2014a,b). Compositional and mode isopleths for all phases were calculated using the software TCIInvestigator (Pearce et al., 2015). The identification of the aluminosilicates was verified using Raman spectrometry. Additional information on the workflow with relevant background and methodology are provided in Korhonen et al. (2020).

Results

Metamorphic *P–T* estimates have been derived based on detailed examination of two thin sections and the bulk-rock composition. The *P–T* pseudosection for this sample was calculated over a *P–T* range of 2–10 kbar and 650–800 °C (Fig. 4). The solidus is H₂O-saturated below 4.4 kbar and is located between 675 and 770 °C across the range of modelled pressures. At pressures above 4.4 kbar, muscovite is consumed at temperatures just above the solidus. At temperatures above 750 °C garnet is stable across all modelled pressures, and has a minimum stability of 6.3 kbar between 650 and 730 °C. Cordierite is stable at low pressures, i.e. below 2 kbar at 650 °C and below 5.4 kbar at 800 °C. Aluminosilicate-absent assemblages are stable at lower pressures.

Table 1. Biotite compositions for sample 212305: andalusite–sillimanite pelitic migmatite, Mount Joseph

<i>Setting^(a)</i>	<i>Fol</i>	<i>Fol</i>	<i>Fol</i>	<i>CM</i>	<i>CM</i>	<i>CM</i>	<i>CM</i>	<i>P</i>	<i>P</i>	<i>P</i>	<i>P</i>	<i>P</i>	<i>P</i>	<i>P</i>	<i>Rims</i>	<i>Rims</i>	<i>Rims</i>	<i>Rims</i>
<i>wt%</i>																		
SiO ₂	34.87	34.04	33.64	33.93	34.92	33.98	33.06	32.67	33.49	33.75	32.74	33.63	34.38	33.44	33.92	33.77	33.71	34.27
TiO ₂	1.52	1.59	1.73	2.69	2.18	2.59	2.13	2.71	2.82	2.76	2.79	2.99	2.99	2.97	2.65	2.63	2.54	2.64
Al ₂ O ₃	19.90	19.81	19.13	19.45	27.14	19.16	26.86	18.65	18.70	18.85	18.62	18.69	19.21	19.45	19.36	19.29	19.38	19.17
Cr ₂ O ₃	0.01	0.03	0.06	0.03	0.01	0.02	0.03	0.02	0.01	0.02	0.05	0.00	0.00	0.06	0.01	0.00	0.01	0.02
FeO	21.15	21.15	22.40	22.24	17.75	22.40	18.23	21.59	22.36	21.88	21.31	21.57	21.86	22.26	21.79	22.09	21.83	22.44
MnO	0.07	0.07	0.10	0.11	0.07	0.09	0.08	0.09	0.10	0.07	0.10	0.09	0.07	0.09	0.08	0.10	0.07	0.10
MgO	7.70	7.47	7.09	6.77	5.61	6.53	5.21	6.65	6.69	6.72	6.50	6.71	6.76	5.44	6.70	6.73	6.98	6.83
ZnO	0.00	0.02	0.06	0.00	0.05	0.04	0.03	0.04	0.01	0.00	0.01	0.05	0.00	0.06	0.05	0.02	0.09	0.02
CaO	0.07	0.04	0.01	0.00	0.01	0.00	0.01	1.17	0.00	0.02	0.02	0.04	0.01	0.05	0.02	0.02	0.01	0.01
Na ₂ O	0.16	0.14	0.14	0.13	0.11	0.13	0.14	0.13	0.13	0.09	0.17	0.18	0.16	0.10	0.17	0.15	0.15	0.09
K ₂ O	9.27	9.48	9.51	9.58	7.87	9.46	7.79	9.21	9.49	9.38	9.37	9.32	9.45	8.99	9.42	9.44	9.54	9.44
Cl	0.01	0.00	0.00	0.00	0.00	0.01	0.01	0.00	0.01	0.01	0.01	0.01	0.01	0.01	0.01	0.01	0.01	0.00
F	0.36	0.29	0.27	0.28	0.32	0.27	0.21	0.27	0.28	0.26	0.27	0.35	0.30	0.28	0.30	0.30	0.29	0.26
H ₂ O	3.73	3.71	3.68	3.73	3.94	3.71	3.86	3.64	3.67	3.69	3.60	3.64	3.74	3.65	3.70	3.70	3.71	3.75
Total	98.83	97.84	97.84	98.97	99.99	98.37	97.66	96.82	97.76	97.49	95.54	97.28	98.93	96.84	98.17	98.25	98.30	99.03
Oxygen	11	11	11	11	11	11	11	11	11	11	11	11	11	11	11	11	11	11
Si	2.67	2.65	2.64	2.62	2.55	2.64	2.49	2.59	2.63	2.65	2.62	2.64	2.65	2.64	2.64	2.63	2.62	2.65
Ti	0.09	0.09	0.10	0.16	0.12	0.15	0.12	0.16	0.17	0.16	0.17	0.18	0.17	0.18	0.15	0.15	0.15	0.15
Al	1.80	1.81	1.77	1.77	2.34	1.76	2.39	1.74	1.73	1.74	1.76	1.73	1.74	1.81	1.77	1.77	1.78	1.74
Cr	0.00	0.00	0.00	0.00	0.00	0.00	0.00	0.00	0.00	0.00	0.00	0.00	0.00	0.00	0.00	0.00	0.00	0.00
Fe ^{3+(b)}	0.07	0.07	0.07	0.07	0.05	0.07	0.06	0.07	0.07	0.07	0.07	0.07	0.07	0.07	0.07	0.07	0.07	0.07
Fe ²⁺	1.29	1.31	1.40	1.37	1.03	1.38	1.09	1.36	1.39	1.36	1.36	1.35	1.34	1.40	1.35	1.37	1.35	1.38
Mn ²⁺	0.00	0.00	0.01	0.01	0.00	0.01	0.01	0.01	0.01	0.00	0.01	0.01	0.00	0.01	0.01	0.01	0.00	0.01
Mg	0.88	0.86	0.83	0.78	0.61	0.76	0.59	0.79	0.78	0.79	0.78	0.79	0.78	0.64	0.78	0.78	0.81	0.79
Zn	0.00	0.00	0.00	0.00	0.00	0.00	0.00	0.00	0.00	0.00	0.00	0.00	0.00	0.00	0.00	0.00	0.01	0.00
Ca	0.01	0.00	0.00	0.00	0.00	0.00	0.00	0.10	0.00	0.00	0.00	0.00	0.00	0.00	0.00	0.00	0.00	0.00
Na	0.02	0.02	0.02	0.02	0.02	0.02	0.02	0.02	0.02	0.01	0.03	0.03	0.02	0.01	0.02	0.02	0.02	0.01
K	0.91	0.94	0.95	0.94	0.73	0.94	0.75	0.93	0.95	0.94	0.96	0.93	0.93	0.91	0.93	0.94	0.95	0.93
Cl	0.00	0.00	0.00	0.00	0.00	0.00	0.00	0.00	0.00	0.00	0.00	0.00	0.00	0.00	0.00	0.00	0.00	0.00
F	0.09	0.07	0.07	0.07	0.07	0.07	0.05	0.07	0.07	0.06	0.07	0.09	0.07	0.07	0.08	0.07	0.07	0.06
OH-	1.91	1.93	1.93	1.93	1.93	1.93	1.95	1.93	1.93	1.94	1.93	1.91	1.93	1.93	1.92	1.93	1.93	1.94
Total	7.73	7.76	7.79	7.75	7.47	7.73	7.52	7.78	7.75	7.73	7.75	7.72	7.71	7.67	7.73	7.74	7.76	7.73
<i>Compositional variables^(c)</i>																		
XFe	0.59	0.60	0.63	0.64	0.63	0.65	0.65	0.63	0.64	0.63	0.64	0.63	0.63	0.69	0.63	0.64	0.62	0.64
Al ^{vi}	0.47	0.46	0.40	0.40	0.89	0.40	0.88	0.34	0.36	0.39	0.38	0.37	0.39	0.45	0.41	0.40	0.40	0.39

NOTES: (a) Fol, within fibrolite–biotite foliation; CM, coarse grains in matrix; P, within Al₂SiO₅ porphyroblasts; Rims, rims around Al₂SiO₅ porphyroblasts
(b) Fe³⁺ contents assumed to be 10% of Fe total
(c) XFe = Fe²⁺/(Fe²⁺ + Mg); Al^{vi} = Al cations on tetrahedral site

Biotite shows a range of compositions that can be grouped based on microstructural settings (Table 1, Appendix). Biotite included within and mantling aluminosilicate porphyroblasts contain the highest Ti contents of 0.15 – 0.18 per formula unit (pfu) and $X_{Fe} [= Fe^{2+}/(Fe^{2+} + Mg)]$ contents of 0.625 – 0.64, with a single analysis having $X_{Fe} = 0.69$. Biotite intergrown with fibrolite within the foliation has the lowest Ti contents (= 0.09 – 0.10 pfu) and lowest X_{Fe} contents (= 0.59 – 0.63). Coarse-grained biotite within the matrix has variable compositions, ranging from compositions similar to the biotite associated with aluminosilicate porphyroblasts to eastonite-rich compositions with lower Ti contents of 0.12.

Table 2. Measured whole-rock and modelled compositions for sample 212305: andalusite–sillimanite pelitic migmatite, Mount Joseph

<i>XRF whole-rock composition (wt%)^(a)</i>												
SiO ₂	TiO ₂	Al ₂ O ₃	Fe ₂ O ₃ ^(b)	FeO ^(b)	MnO	MgO	CaO	Na ₂ O	K ₂ O	P ₂ O ₅	LOI	Total
73.78	0.65	13.31	0.78	3.89	0.03	1.41	0.97	0.81	2.35	0.06	1.44	99.48
<i>Normalized composition used for phase equilibria modelling (mol%)</i>												
SiO ₂	TiO ₂	Al ₂ O ₃	O ^(c)	FeO ^(d)	MnO	MgO	CaO	Na ₂ O	K ₂ O	–	H ₂ O ^(e)	Total
78.56	0.52	8.35	0.31	4.09	0.03	2.24	1.11	0.83	1.59	–	2.36	100

NOTES: (a) Data and analytical details are available from the WACHEM database <<http://geochem.dmp.wa.gov.au/geochem/>>
(b) FeO analysed by Fe²⁺ titration; Fe₂O₃ content calculated by difference
(c) O content (for Fe₂O₃) based on titration value
(d) FeO² = moles FeO + 2 * moles O
(e) H₂O content reduced from measured LOI, see text for further details

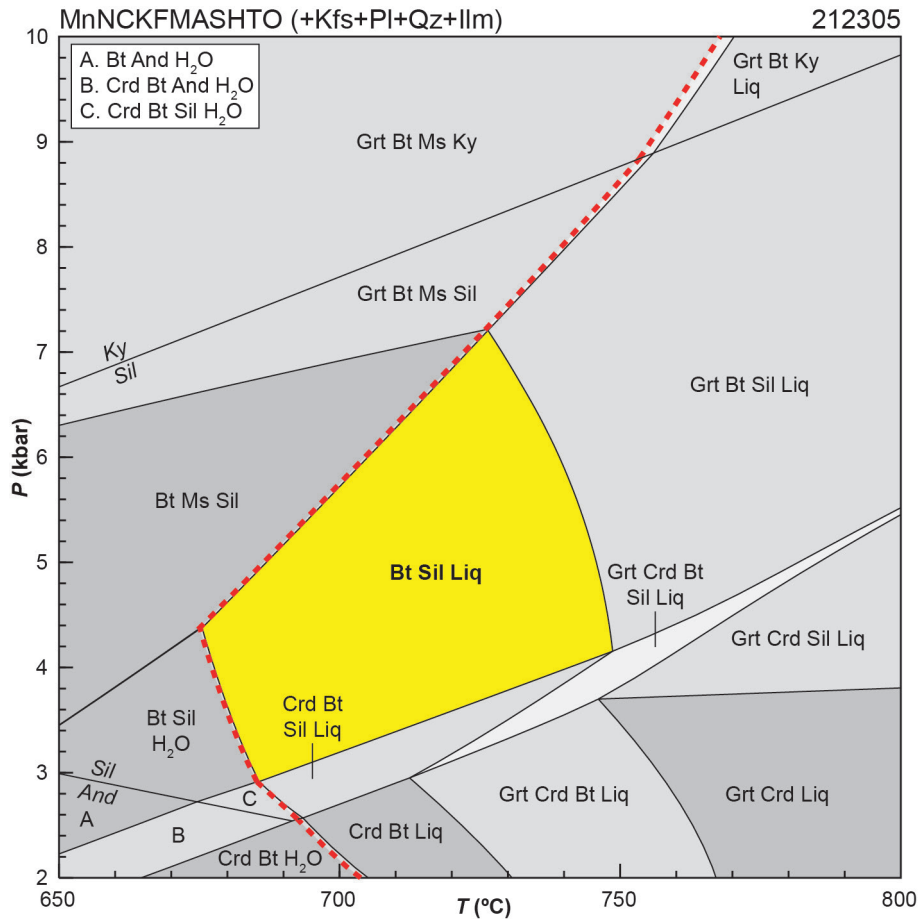


Figure 4. *P–T* pseudosection calculated for sample 212305: andalusite–sillimanite pelitic migmatite, Mount Joseph. Assemblage field corresponding to peak metamorphic conditions is shown in bold text and yellow shading. Red dashed line represents the solidus. Abbreviations: And, andalusite; Bt, biotite; Crd, cordierite; Grt, garnet; H₂O, fluid (pure H₂O); Ilm, ilmenite; Kfs, K-feldspar; Ky, kyanite; Liq, silicate melt; Opx, orthopyroxene; Pl, plagioclase; Qz, quartz; Sil, sillimanite

Interpretation

Based on the coarser grain size and mineral associations that support textural equilibrium, the peak metamorphic assemblage is inferred to be biotite–sillimanite–K-feldspar–plagioclase–quartz–ilmenite–melt. The sparse muscovite preserved in the sample is interpreted to be mostly relic grains that were not completely consumed during melting. Andalusite is interpreted to partially replace coarse-grained sillimanite porphyroblasts during a separate event at lower grade conditions, which was likely synchronous with the development of the fibrolite–biotite foliation. The growth of metastable fibrolite at P – T conditions within the andalusite stability field is well recognized (e.g. Kerrick, 1987) and commonly forms through the breakdown of biotite in the presence of fluids. This interpretation is also consistent with the Ti content of biotite associated with these different petrographic settings. Biotite within and mantling the aluminosilicate porphyroblasts have higher Ti contents than the biotite intergrown with fibrolite in the foliation, indicating that the growth of biotite within the porphyroblasts occurred at higher temperatures than the biotite within the foliation (Appendix).

The inferred peak metamorphic assemblage of biotite–sillimanite–K-feldspar–plagioclase–quartz–ilmenite–melt is stable between 675 and 750 °C at 2.9 – 7.2 kbar. The peak field is delimited by the stability of garnet at higher temperature, the stability of cordierite at lower pressure, and the solidus at lower temperature and higher pressure. A sample of cordierite-bearing pelitic migmatite located 1.7 km to the west yields peak P – T estimates of 2.7 – 4.4 kbar and 680–755 °C (GSWA 212316, preliminary data). There are no obvious

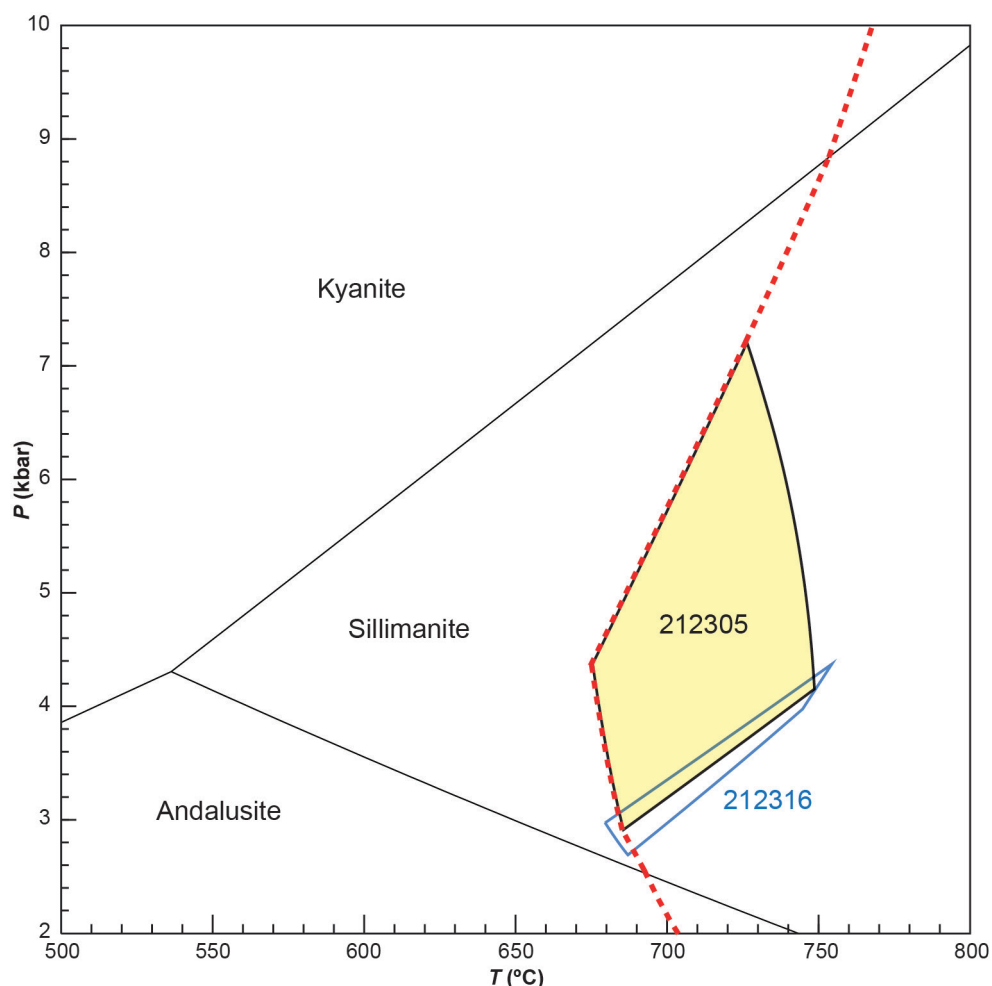


Figure 5. Summary diagram for sample 212305: andalusite–sillimanite pelitic migmatite, Mount Joseph. Assemblage field corresponding to peak metamorphic conditions is shown in light yellow shading (see Fig. 4). Red dashed line represents the solidus. Peak metamorphic conditions from a sample 1.7 km to the west is shown in blue (GSWA 212316). The close proximity of these samples and the potential overlap of peak conditions may indicate peak pressures less than 4 kbar. The aluminosilicate phase diagram is also shown to highlight that the growth of andalusite after sillimanite occurs at lower temperatures

structures between these samples, and overlaying the P – T results from the two samples suggests that peak pressures for the sample reported may have been near the lower pressure limit of the peak assemblage field (Fig. 5). The conditions of the growth of andalusite are not well constrained, but must have occurred within the andalusite stability field at lower temperatures (Fig. 5). The timing of peak metamorphism is dated at 1854 ± 4 Ma, constrained by Group M monazite that occurs within aluminosilicate porphyroblasts and surrounding coarse-grained biotite. The growth of andalusite and development of the fibrolite–biotite foliation is dated at 1823 ± 6 Ma from Group M2 monazite within the biotite–fibrolite foliation. It is not clear whether the growth of andalusite was a separate thermal event or part of the cooling history following peak metamorphism. However, andalusite replacing sillimanite is generally not a common relationship observed in rocks, and in this case it is attributed to an influx of fluids during deformation within the andalusite stability field.

Peak metamorphic conditions are estimated at 675–750 °C and 2.9 – 7.2 kbar, with an apparent thermal gradient between 100 and 235 °C/kbar. Metamorphic constraints from a nearby sample record peak pressures less than 4 kbar, corresponding to thermal gradients above 180 °C/kbar. Muscovite is interpreted to be relic, suggesting that the prograde segment of the P – T path passed through muscovite stability. However, the bulk composition used for the modelling (Fig. 4) underwent melting and potentially melt loss, therefore it cannot be used to constrain the prograde trajectory. It is also not clear if the andalusite represents part of a single retrograde path or a separate fluid-mediated event; therefore, the overall shape of the P – T path is not defined.

References

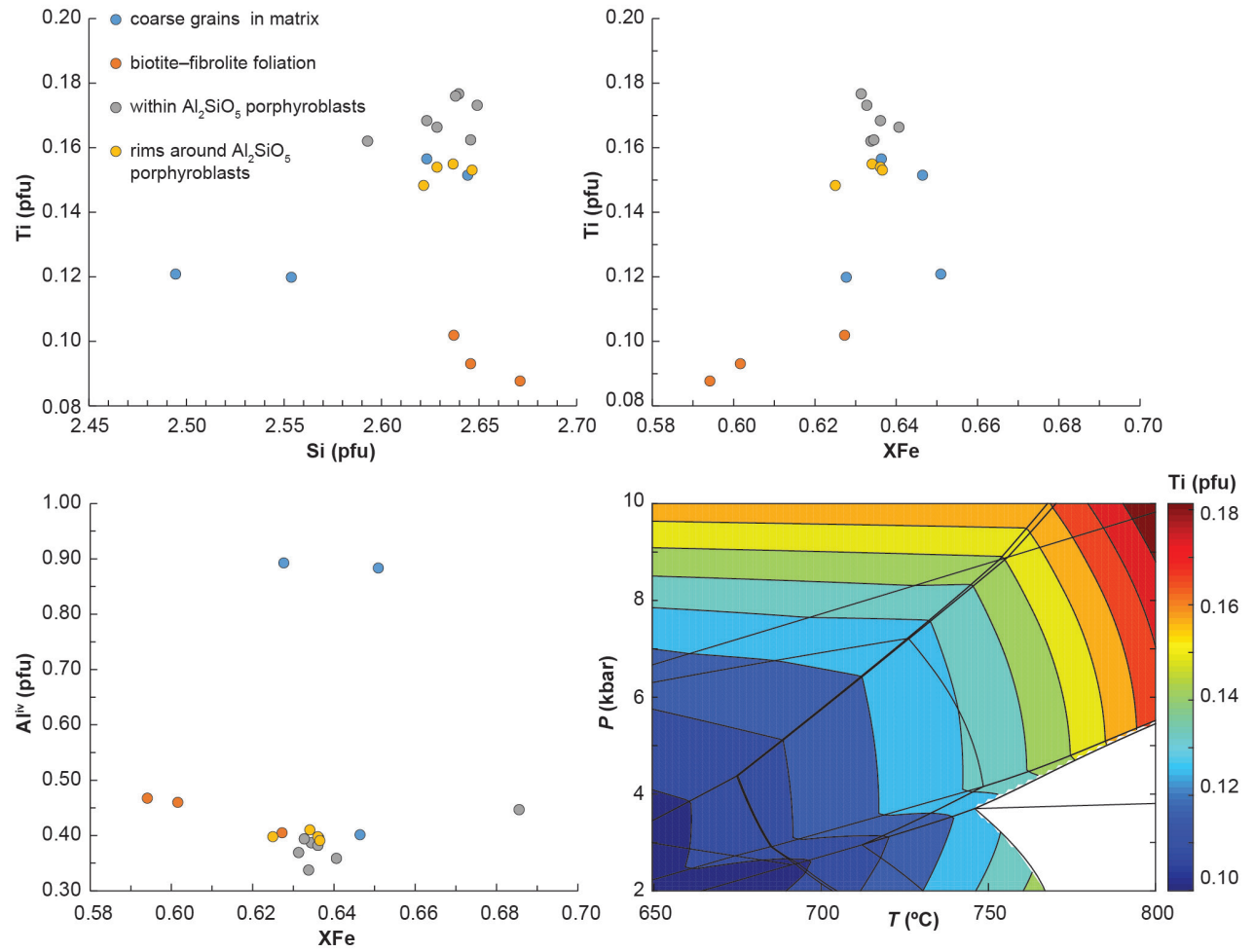
- Fielding, IOH, Wingate, MTD, Lu, Y, Korhonen, FJ and Hollis, JA 2019a, 212305: pelitic migmatite, Mount Joseph; Geochronology Record 1620: Geological Survey of Western Australia, 6p.
- Fielding, IOH, Wingate, MTD, Lu, Y, Korhonen, FJ and Hollis, JA 2019b, 212316: pelitic migmatite, Mount Joseph; Geochronology Record 1623: Geological Survey of Western Australia, 5p.
- Fielding, IOH, Wingate, MTD, Lu, Y, and Hollis, JA 2020, 212317: pelitic migmatite, Mount Joseph; Geochronology Record 1624: Geological Survey of Western Australia, 8p.
- Griffin, TJ, Page, RW, Sheppard, S and Tyler, IM 2000, Tectonic implications of Palaeoproterozoic post-collisional, high-K felsic igneous rocks from the Kimberley region of northwestern Australia: *Precambrian Research*, v. 101, p. 1–23.
- Holland, TJB and Powell, R 2011, An improved and extended internally consistent thermodynamic dataset for phases of petrological interest, involving a new equation of state for solids: *Journal of Metamorphic Geology*, v. 29, no. 3, p. 333–383.
- Kerrick, DM 1987, Fibrolite in contact aureoles of Donegal, Ireland: *American Mineralogist*, v. 72, p. 240–254.
- Korhonen, FJ, Kelsey, DE, Fielding IOH and Romano, SS 2020, The utility of the metamorphic rock record: constraining the pressure–temperature–time conditions of metamorphism: Geological Survey of Western Australia, Record 2020/14, 24p.
- Pearce, MA, White, AJR and Gazley, MF 2015, TCInvestigator: automated calculation of mineral mode and composition contours for thermocalc pseudosections: *Journal of Metamorphic Geology*, v. 33, no. 4, p. 413–425, doi:10.1111/jmg.12126.
- Phillips, C, de Souza Kovacs, N and Hollis, JA 2015, Richenda, WA Sheet 3963: Geological Survey of Western Australia: 1:100 000 Geological Series.
- Powell, R and Holland, TJB 1988, An internally consistent dataset with uncertainties and correlations: 3. Applications to geobarometry, worked examples and a computer program: *Journal of Metamorphic Geology*, v. 6, no. 2, p. 173–204.
- Tyler, IM, Page, RW and Griffin, TJ 1999, Depositional age and provenance of the Marboo Formation from SHRIMP U–Pb zircon geochronology: implications for the early Palaeoproterozoic tectonic evolution of the Kimberley region, Western Australia: *Precambrian Research*, v. 95, p. 225–243.
- White, RW, Powell, R, Holland, TJB, Johnson, TE and Green, ECR 2014a, New mineral activity–composition relations for thermodynamic calculations in metapelitic systems: *Journal of Metamorphic Geology*, v. 32, no. 3, p. 261–286.
- White, RW, Powell, R and Johnson, TE 2014b, The effect of Mn on mineral stability in metapelites revisited: New a – x relations for manganese-bearing minerals: *Journal of Metamorphic Geology*, v. 32, no. 8, p. 809–828.

Links

Metamorphic history introduction document: Intro_2020.pdf

Appendix

Biotite compositional data from sample 212305: andalusite–sillimanite pelitic migmatite, Mount Joseph, obtained by electron probe microanalyser (EPMA). Full compositional data provided in Table 1. Labelled P – T pseudosection shown on Figure 4. pfu, cations per formula unit based on 11 oxygens; $X_{Fe} = Fe^{2+}/(Fe^{2+} + Mg)$



Recommended reference for this publication

Korhonen, FJ, Romano, SS, Fielding, IOH, Kelsey, DE and Hollis, JA 2022, 212305: andalusite–sillimanite pelitic migmatite, Mount Joseph; Metamorphic History Record 13: Geological Survey of Western Australia, 9p.

Data obtained: 6 November 2018

Date released: 14 April 2022

This Metamorphic History Record was last modified on 29 March 2022.

Grid references in this publication refer to the Geocentric Datum of Australia 1994 (GDA94). All locations are quoted to at least the nearest 100 m.

WAROX is GSWA's field observation and sample database. WAROX site IDs have the format 'ABCXXXnnnnnnSS', where ABC = geologist username, XXX = project or map code, nnnnnn = 6 digit site number, and SS = optional alphabetic suffix (maximum 2 characters).

Isotope and element analyses are routinely conducted using the GeoHistory laser ablation ICP-MS and Sensitive High-Resolution Ion Microprobe (SHRIMP) ion microprobe facilities at the John de Laeter Centre (JdLC), Curtin University, with the financial support of the Australian Research Council and AuScope National Collaborative Research Infrastructure Strategy (NCRIS). The Tescan Integrated Mineral Analyser (TIMA) instrument was funded by a grant from the Australian Research Council (LE140100150) and is operated by the JdLC with the support of the Geological Survey of Western Australia, The University of Western Australia (UWA) and Murdoch University. Mineral analyses are routinely obtained using the electron probe microanalyser (EPMA) facilities at the Centre for Microscopy, Characterisation and Analysis at UWA, and at Adelaide Microscopy, University of Adelaide.

Digital data related to WA Geology Online, including geochronology and digital geology, are available online at the Department's Data and Software Centre and may be viewed in map context at GeoVIEW.WA.

Disclaimer

This product uses information from various sources. The Department of Mines, Industry Regulation and Safety (DMIRS) and the State cannot guarantee the accuracy, currency or completeness of the information. Neither the department nor the State of Western Australia nor any employee or agent of the department shall be responsible or liable for any loss, damage or injury arising from the use of or reliance on any information, data or advice (including incomplete, out of date, incorrect, inaccurate or misleading information, data or advice) expressed or implied in, or coming from, this publication or incorporated into it by reference, by any person whosoever.



© State of Western Australia (Department of Mines, Industry Regulation and Safety) 2022

With the exception of the Western Australian Coat of Arms and other logos, and where otherwise noted, these data are provided under a Creative Commons Attribution 4.0 International Licence. (<http://creativecommons.org/licenses/by/4.0/legalcode>)

Further details of geoscience products are available from:

Information Centre
Department of Mines, Industry Regulation and Safety
100 Plain Street
EAST PERTH WA 6004
Telephone: +61 8 9222 3459 | Email: publications@dmirs.wa.gov.au
www.dmirs.wa.gov.au/GSWApublications